Potential of novel porous materials for capture of toluene traces in air under humid conditions

Quentin Pujol, Guy Weber, Jean-Pierre Bellat, Sven Grätz, Annika Krusenbaum, Lars Borchardt, Igor Bezverkhyy

Potential of novel porous materials for capture of toluene traces in air under humid conditions

Quentin Pujol[a], Guy Weber[a], Jean-Pierre Bellat[a], Sven Grätz[b], Annika Krusenbaum[b], Lars Borchardt[b], Igor Bezverkhyy[a]*

[a] Laboratoire Interdisciplinaire Carnot de Bourgogne, UMR 6303 CNRS-Université de Bourgogne Franche-Comté, BP 47870, 21078 Dijon Cedex, France

[b] Inorganic Chemistry I, Ruhr-Universität Bochum, Universitätsstraße 150, 44801 Bochum, Germany

* Corresponding author, email: igor.bezverkhyy@u-bourgogne.fr, tel. + 33 380396038, fax +33 380396132

Abstract

We evaluated the potential of several novel porous materials for toluene capture in air under humid conditions. Four novel porous solids of different nature were studied and compared to two reference materials: two hyper-cross-linked polymers HCP and SMP, the metal organic framework MAF-6 and the activated carbon derived from MAF-6 (AC-MAF-6) with references (Norit RB3 and a dealuminated Y zeolite (DAY)). The affinity of the sorbents for toluene was determined from adsorption isotherms recorded at 25 °C and the low pressure part of the isotherms (< 100 Pa) were successfully fitted with the Unilan equation allowing extrapolation to sub ppm (< 0.1 Pa) concentration range. These equilibrium measurements were complemented by recording the breakthrough curves at 10 Pa of toluene under dry and humid conditions (50 % relative humidity). While MAF-6 and DAY show low dynamic capacities under these conditions, HCP and AC-MAF-6 exhibit much better performances which in the case of AC-MAF-6 are close to RB3 activated carbon even under humid conditions. Moreover, these sorbents can be successfully regenerated under mild conditions (200°C) and show stable performance through adsorption/desorption cycles. Our work suggests that HCP and MAF-6-derived activated carbon are promising materials for toluene capture in air under realistic conditions.

Keywords: toluene adsorption, BTEX capture, hyper-cross-linked polymers, MOF-derived carbon

1. Introduction

Among all volatile organic compounds (VOCs), aromatic substances are one of the most frequently encountered groups in the outdoor and indoor air. The main compounds in this group are BTEX (benzene, toluene, ethylbenzene and xylenes) which originates from different sources. While in outdoor air the main source is the combustion and evaporation of the liquid fuels [1], indoors BTEX compounds are emitted by numerous products such as household cleaners, fabric and leather treatments, automotive products, adhesives and paints [2,3].

The acute and chronic toxicity of BTEX compounds for humans is well documented [4-7]. Thus benzene is listed as a Group 1 carcinogen [8] and toluene has reproductive toxicity and neurotoxicity [5]. Because of these effects the stringent norms on BTEX concentration are imposed by regulatory bodies in the context of the occupational health. Thus the exposure limits recommended by the U.S. National Institute for Occupational Safety and Health (NIOSH) is 0.1 ppm for benzene and 100 ppm for toluene. The recommended values for general public are even more stringent: 9 ppb for benzene and 5 ppm for toluene (U.S. Environmental Protection Agency reference concentrations [2]).

Different technologies were proposed to remove BTEX compounds from air to achieve these concentrations [9,10]. The thermal oxidation is currently used on the industrial scale to purify the industrial waste gases containing high concentration of BTEX and other VOCs (> 1000 ppm). However, this technology is not suitable for treatment of ambient air in which the concentration is much lower (< 10 ppm). In these cases the adsorption on activated carbon-based materials were shown to be the most efficient approach [10,11]. Despite the high efficiency of active carbon, it has some shortcomings such as flammability or limited on site regeneration. That is why other types of conventional porous materials, e. g. zeolites or mesoporous silicas, were also studied [12-15].

In addition to these traditional sorbents, various novel porous materials have been intensively studied in BTEX capture. Thus, some metal organic frameworks (MOF) were shown to possess promising properties under conditions relevant for indoor air purification [16-18]. Beside their direct application

as sorbents, MOFs can also be used as precursors for another class of advanced porous materials – MOF-derived carbons possessing exceptional textural properties and tunable surface chemistry [19]. Recently it has been shown that MOF-derived carbons outperform traditional activated carbons in toluene capture under humid conditions [20,21]. Hyper-cross-linked polymers based on covalent bonds between various aromatic units are another example of recently discovered microporous materials. Due to their strong hydrophobicity and high surface areas they demonstrate promising properties in adsorption of aromatic compounds [22-26].

The present work continues exploration of novel porous materials in BTEX capture using toluene as a representative compound. Several criteria determined our choice of the porous materials for this study. First, the pore size should be sufficiently large to admit toluene molecules having the size of 5.25 Å [27]. Second, we restrained our choice to hydrophobic sorbents since the humidity is ubiquitous in ambient air. Third, the potential use of these materials on a large scale precludes the use of materials whose structure is based on non-commercial ligands prepared through multi-step synthetic procedures. Application of these three criteria led us to choose the following sorbents. First of them is a MOF material known as MAF-6 whose framework is formed by connection between Zn^{2+} and 4-ethylimidazolate ligands. MAF-6 shows strong hydrophobicity and has a cubic structure similar to RHO zeolite with a large cavity (~ 18.4 Å) and the aperture size of 7.6 Å [28] (Fig.S1). The other two studied materials belong to the group of hyper-cross-linked polymers and were prepared by simple mechanochemical reactions. The first one (HCP) is obtained by condensation of (4,4'-bis(chloromethyl)-1,1'-biphenyl) [29] and the second one (SMP) from 1,3,5 – triphenylbenzene [30] (Fig. S1). These materials are rich in aromatic rings, they possess high surface areas and show good thermal stabilities. In addition to molecular type materials we included in our study an activated carbon produced by decomposition of MAF-6 MOF [31-32]. Such materials are similar to conventional active carbons, but due to the presence of nitrogen atoms they are more polar [33]. For

comparison we also studied the properties of two classical toluene sorbents: Norit RB3 activated carbon and a dealuminated zeolite Y (DAY).

Concerning the used methodology, we tried to avoid the main pitfall of many studies in this domain - the use of unrealistic conditions. Indeed, it was shown in [11,34,35] that majority of works dealing with the adsorption of VOCs on the novel materials use too high concentrations. Moreover, they do not provide sufficient information allowing to extrapolate the obtained adsorption capacities to the pressure range relevant to VOCs capture in ambient air. In the present study, to approach the conditions of indoor air purification we evaluated the properties of the sorbents at low toluene pressure: the high-resolution toluene adsorption isotherms were measured down to 0.1 Pa (~ 1 ppm). In addition, we fitted the obtained isotherms by the Unilan model which has a thermodynamically consistent (linear) behavior at the zero-pressure limit. The use of this model allowed us to predict the adsorption capacities in the pressure range that is not accessible experimentally. This characterization under static equilibrium conditions was complemented by dynamic measurements of the breakthrough curves under 10 Pa of toluene in the presence of 50 % of relative humidity (RH). Finally, desorption of toluene was studied in order to evaluate the regenerability of the most efficient sorbents.

2. Experimental

2.1. Materials

Norit RB3 activated carbon and cyclohexane were purchased from Sigma-Aldrich. $Zn(NO_3)_2 \cdot 6H_2O$ and aqueous ammonia solution (> 28 wt.%) were provided by ROTH. 2-ethylimidazole was purchased from Alfa Aesar. DAY (dealuminated faujasite zeolite, composition - $Na_2Al_2Si_{190}O_{384}$) was provided by Degussa.

Both hyper-cross-linked polymers were synthesized by liquid assisted mechanochemical reaction. The synthesis of HCP was accomplished in accordance to a published synthesis procedure [29].

During the reaction, 0.821 g (3.27 mmol, 1 eq) 4,4'-bis(chloromethyl)-1,1'-biphenyl, 3.179 g (19.61 mmol, 6 eq) $FeCl_3$ and 1 mL dibromomethane were milled for 35 min at 500 rpm in a Fritsch Pulverisette 7 planetary ball mill. As grinding auxiliaries, 22 zirconium oxide milling balls and a 45 mL beaker of the same material were utilized. After the reaction was completed, the product was washed with 200 mL of water and 100 mL of ethanol, respectively, and dried at 80 °C overnight.

In a similar fashion, the synthesis of SMP was adapted from the literature [30]. A 50 mL zirconium oxide milling vessel was equipped with 22 zirconium oxide milling balls, 0.540 g (1.77 mmol, 1 eq) 1,3,5-triphenylbenzene, 3.460 g (21.33 mmol, 12 eq) $FeCl_3$ and 1 mL dichloromethane. The mixture was milled for 5 minutes at 30 Hz in a Retsch MM500 mixer mill. Afterwards, the product was washed with 200 mL of water and 100 mL of acetone and dried at 80 °C overnight.

MAF-6 was prepared according to the published procedure [28] with minor changes. First, $Zn(OH)_2$ was prepared from $Zn(NO_3)_2$: zinc nitrate hexahydrate (1.16 g, 3.9 mmol, 1 eq) was dissolved in 10 mL of water and 0.585 mL of concentrated ammonia solution (7.8 mmol, 2 eq) was added. The resulting precipitate was washed 3 times with 10 mL of water and centrifuged at 5000 rpm. Then, the freshly prepared $Zn(OH)_2$ was dissolved in 19.5 mL of concentrated ammonia (260 mmol, 66 eq). This solution was poured into the ligand solution consisting of 0.751 g (7.8 mmol, 2 eq) of 2-ethylimidazole in 54.6 mL of ethanol and 3.9 mL of cyclohexane which was added just before mixing two solutions. The obtained suspension was stirred at room temperature for 30 minutes then filtered and washed with ethanol (30 mL). The XRD pattern of the obtained solid matches well the theoretical pattern of MAF-6 (Fig.S2).

The activated carbon AC-MAF-6 was prepared according to [31] by thermal decomposition of MAF-6 in a tubular furnace under N_2 flow at 1000 °C for 24 h followed by washing of the obtained active carbon in 1M HCl solution.

2.2. Characterization techniques

N_2 adsorption-desorption isotherms at 77.4 K were measured using ASAP2020 instrument from Micromeritics. Prior to measurements the samples were degassed under secondary vacuum (< 10^{-4} hPa) at 200 °C for 4 h. The BET surface areas were calculated from the isotherms following the recommendations suggested in [36]. The microporous volume was determined using the t-plot. The total pore volume was calculated from the amount adsorbed at P/P^0 = 0.99 and the mesoporous volume was estimated from the difference between the total pore volume and the micropore volume. The pore size distributions of the samples were calculated using the adsorption branch by NLDFT approach implemented in the SAIEUS software [37]. 2D-NLDFT heterogeneous surface model for N_2 in carbon was used in the calculations for activated carbons and hyper-cross-linked polymers. For DAY the model for zeolite H-form was applied.

Thermal gravimetric analysis (TGA) was done using a SETARAM Sensys Evo apparatus. The samples were heated under flow of O_2/N_2 (20/80) mixture at 5 °/min up to 700 °C.

Scanning electron microscopy (SEM) images were taken on HITACHI SU8230 microscope or on JEOL JSM7600F. The samples were dispersed on a carbon scotch and metallized with Cr (HITACHI) or with carbon (JEOL).

XRD patterns were recorded on diffractometer Bruker D8-A25 Discover equipped with a LynxEye XE detector using Cu Kα radiation.

The X-ray photoelectron spectra (XPS) were recorded on PHI 5000 Versaprobe apparatus using Al Kα radiation. The powdered samples were pressed onto a sheet of indium. The XPS spectra were treated using CasaXPS software [38].

2.3. Adsorption measurements under equilibrium conditions

Toluene and water adsorption/desorption isotherms were measured by thermogravimetry (McBain type thermobalance) under controlled vapor pressure. The homemade experimental set-up is

described in detail in [39]. The sample (*ca.*15 mg) is first evacuated in situ under dynamic vacuum (10^{-5} hPa) for 16 h at 200°C. Then, the sample is cooled down to room temperature and the adsorption/desorption isotherms are measured step-by-step using a static method by introducing successively toluene or water vapor doses into the thermobalance. Once a constant mass is reached, the next equilibrium state is achieved by increasing the vapor pressure. After saturation of the sample the vapor pressure is decreased step by step by pumping to measure the desorption branch of the isotherm. All adsorption/desorption isotherms were measured at 25 °C within the vapor pressure range from 10^{-4} to about 37 hPa (toluene) or 30 hPa (water).

2.4. Breakthrough curves measurements under dry and humid atmosphere

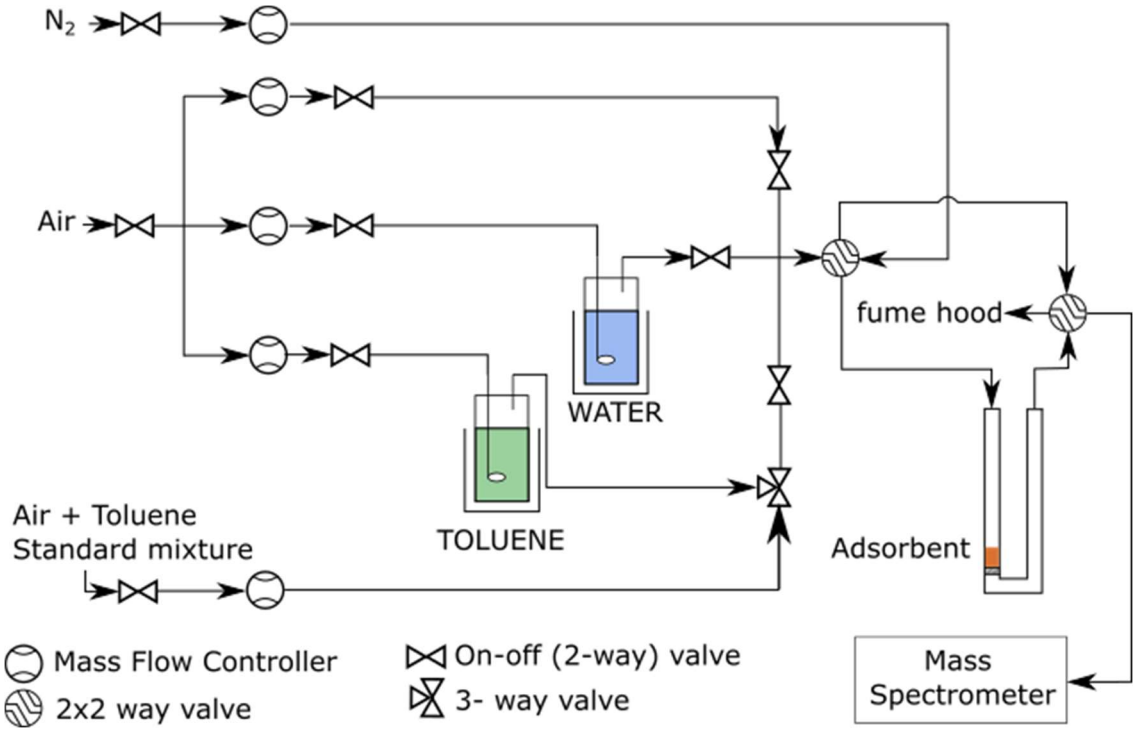

Figure 1 Scheme of the setup for the breakthrough curve measurements.

For breakthrough curves measurements Norit RB3 carbon (delivered in the form of extrudates) was crushed and sieved to obtain the fraction 90 – 125 μm. Powdered DAY was compacted using a press

into tablets which were crushed and sieved between 280 and 320 μm. This particle size was chosen in order to decrease the pressure drop which was too high with 100 μm particles. The other samples were used in a powdered form without any shaping.

Toluene breakthrough curves were measured using a home-built setup (Fig.1). The solids were placed in a pyrex U-shaped reactor (internal diameter – 6 mm) and their mass was adjusted in order to obtain the bed height of 1 cm (70 – 130 mg depending on solid). Before measuring the breakthrough curves the samples were activated under N_2 flow at 200 °C for 4 h.

For measurements of toluene breakthrough curves first the carrier gas flow (cylinder air, 20% O_2 – 80% N_2) was loaded with toluene vapor (500 ppm) using a bubbler cooled to – 39 °C by a cryostat. Then this concentrated flow was diluted either with pure carrier gas (adsorption under dry conditions) or water – saturated carrier gas (adsorption under humid conditions). The humid gas flow was obtained by passing the carrier gas through a bubbler filled with water and immersed into another cryostat. The temperatures of the cryostats and the two carrier gas flows were adjusted to obtain 100 mL/min of flow containing 100 ppm of toluene at 50% of relative humidity which was controlled using a probe from ROTRONIC. The mixture at the reactor outlet was analyzed using an online quadrupole mass spectrometer (Omnistar model from Pfeiffer vacuum). To calibrate the mass spectrometer a standard mixture was used which contained 500 ppm of toluene in 20% O_2 – 80% N_2 mixture (Air Liquide).

The breakthrough curves were used to calculate two parameters characterizing dynamic adsorption process. First one, breakthrough capacity (Q_{bt}) corresponds to the amount of toluene adsorbed before the appearance of 1 ppm of toluene in the flow at the reactor outlet (breakthrough threshold). Second parameter, stoichiometric capacity (Q_{st}) corresponds to the total amount of toluene adsorbed before $C/C_0 = 1$.

To study desorption of toluene, the same setup as for breakthrough curves measurements was used. The activated sample (*ca.* 10 mg) was first saturated under a dry air flow containing 100 ppm of

toluene at 25 °C. Then toluene was desorbed by heating with a linear ramp (10°C/min) up to 300 °C under nitrogen flow.

The regenerability was characterized for all samples. To this end *ca.* 10 mg of activated sorbent was saturated under humid air flow (50% RH) containing 100 ppm of toluene at 25 °C. After this step the sample was regenerated under 20% O_2 – 80% N_2 flow at 200 °C for 4 h (temperature ramp – 5°/ min) and cooled down to 25 °C. This sequence, defined as adsorption – desorption cycle, was repeated up to five times.

3. Results and discussion

3.1. Sample characterization

The thermal stability of the solids was characterized by TGA (Fig.S3). The results show a high thermal stability of the used sorbents in the presence of oxygen. The weight loss below 130 °C corresponds to water desorption and this contribution is higher for RB3 and AC-MAF-6 samples. As can be expected, the highest thermal stability is observed for DAY zeolite which does not show any weight loss up to the maximum used temperature (700 °C). The active carbons and SMP polymer are less thermally stable, but their oxidation starts at ~ 450 °C and therefore their regeneration under air flow at 200 – 250 °C should not alter their properties. MAF-6 and HCP polymer are even less thermally stable than the other studied materials. However, their decomposition starts at ~ 350 °C and it should be possible to regenerate them after toluene adsorption without impairing their structure or composition (see below).

The size and shape of the particles in the used sorbents was characterized by SEM (Fig.S4). MAF-6 crystallites have the size of 100 – 400 nm and show a well-defined shape due to a crystalline nature of this solid. As in the previous studies [31] we observe that the morphology of MAF-6 particles is preserved after its transformation into activated carbon (AC-MAF-6). In the case of polymers the primary globular particles smaller than 100 nm can be distinguished which are assembled in highly

porous agglomerates (Fig.S4). The interstitial voids are also observed in the shaped particles of Norit RB3. Finally, DAY zeolite consists of densely packed small crystallites with a wide size distribution (50 - 500 nm).

The surface elemental composition of the samples used in the work was characterized by XPS (Fig.S5 and Table 1). In DAY only Si and O could be detected on the surface because of extremely low Al and Na content. In MAF-6 the surface composition is close to the bulk one (see data in Fig.S5). The elements present on the surface of the activated carbons and hyper-cross-linked polymers and their content are given in Table 1.

Table 1 Surface elemental composition of the active carbons and hyper-cross-linked polymers determined by XPS and deconvolution of the corresponding peaks. For each element the positions of the peak components and their contributions (in parenthesis) are given.

	C		O		Cl		N	
	at.%	C1s components	at.%	O1s components	at.%	Cl2p[a] components	at.%	N1s components
Norit RB3	96.6	284.5 (65.8) 285.1 (34.2)	3.4	530.8 (51.8) 532.9 (48.2)				
AC-MAF-6	87.9	284.5 (60.9) 285.6 (39.1)	6.2	530.1 (4.4) 532.2 (95.6)			5.9	398.4 (41.5) 400.8 (48.8) 403.6 (9.7)
SMP	95.0	284.5 (92.3) 285.4 (7.7)	1.7	531.9 (69.1) 533.3 (30.9)	3.3	198.4 (5.4) 200.4 (94.6)		
HCP	86.5	284.4 (53.5) 285.8 (46.5)	6.4	532.3 (85.1) 534.8 (14.9)	7.1	200.2 (59.5) 201.4 (41.5)		

[a] For Cl2p spectrum the position of $Cl2p_{3/2}$ component of the doublet is given.

Norit RB3 sample in addition to carbon contains only oxygen while AC-MAF-6 contains also nitrogen (5.5 at.%). SMP and HCP polymers in addition to carbon and oxygen also contain a significant amount of chlorine which achieves its highest concentration (7.1 at.%) in HCP. The origin of this chlorine can be traced to the presence of chlorine atoms in the monomer used for the preparation of HCP material (4,4'-bis(chloromethyl)-1,1'-biphenyl) and for both HCP and SMP partial chlorination can be a side reaction during the polymerization caused by an excess of $FeCl_3$.

In all activated carbons and polymers the main contribution to C1s spectra corresponds to aromatic/graphitic carbon (BE = 284.5 eV) with a less intense peak located in the range 285.1 - 285.8 eV which can be attributed to carbon atoms bonded to heteroatoms O, N or Cl [40]. According to deconvolution of O1s peak the main oxygen containing species in the activated carbons are C-OH and/or C-O-C groups (BE = 532.2 – 532.9 eV) and C=O (BE = 530.1 – 530.9 eV) [40]. A small peak at 534.8 eV observed in HCP corresponds to chemisorbed oxygen and/or water species.

The Cl 2p spectrum in both polymer samples can be represented by a sum of two poorly resolved doublets ($2p_{1/2}$ and $2p_{3/2}$ levels). It follows from the literature data that the nature of chlorine (organic or inorganic) can be determined from the position of the Cl $2p_{3/2}$ peak. Thus, in the inorganic or organometallic compounds the corresponding bonding energy is less than 200 eV, while in the compounds containing C-Cl bonds it is higher than this value [41]. According to this value the positions of the doublets in HCP ($2p_{3/2}$ BE = 200.2 and 201.4 eV) show that only organic chlorine is present in the sample. Similarly, in SMP the major part of chlorine is bonded to carbon ($2p_{3/2}$ BE = 200.4 eV). Only a small fraction of chlorine in SMP (5.4 at. %) corresponds to an inorganic chloride ($2p_{3/2}$ BE = 198.4 eV) originating possibly from $FeCl_3$ used as a catalyst during polymerization.

N1s spectrum in AC-MAF-6 can be described by a sum of three contributions. The most abundant species representing 90.3 % of N1s peak surface are pyridine-like ones (BE = 398.4 eV) and quaternary nitrogen species (BE = 400.8 eV). A minor peak located at 403.6 eV can be ascribed to oxidized nitrogen species [33].

The textural properties of the studied sorbents determined from N_2 adsorption at 77 K are presented in Table 2 and in Fig.2a. Nitrogen adsorption isotherms show pore filling at very low pressure which is characteristic of microporous solids. In addition, for all samples except HCP and SMP a plateau is observed corresponding to the micropore volume filling. The isotherms of HCP and SMP are more complex. In addition to micropore filling they show a continuous increase of nitrogen uptake for $P/P^0 > 0.2$ which corresponds to adsorption in mesopores present in these two sorbents.

Table 2 Textural properties of the materials used in the work.

Sample	BET surface area, $m^2.g^{-1}$	Pore volume, $cm^3.g^{-1}$		
		total[a]	micropores[b]	mesopores[c]
Norit RB3	1150	0.50	0.46	0.04
AC-MAF-6	1160	0.62	0.53	0.09
SMP	930	0.75	0.32	0.43
HCP	1640	1.17	0.57	0.60
MAF-6	1640	0.76	0.65	0.11
DAY	860	0.40	0.31	0.09

[a] Calculated from the N_2 amount adsorbed at $P/P^0 = 0.99$

[b] Determined from the t-plot

[c] Estimated from the difference between the total pore volume and the micropore volume

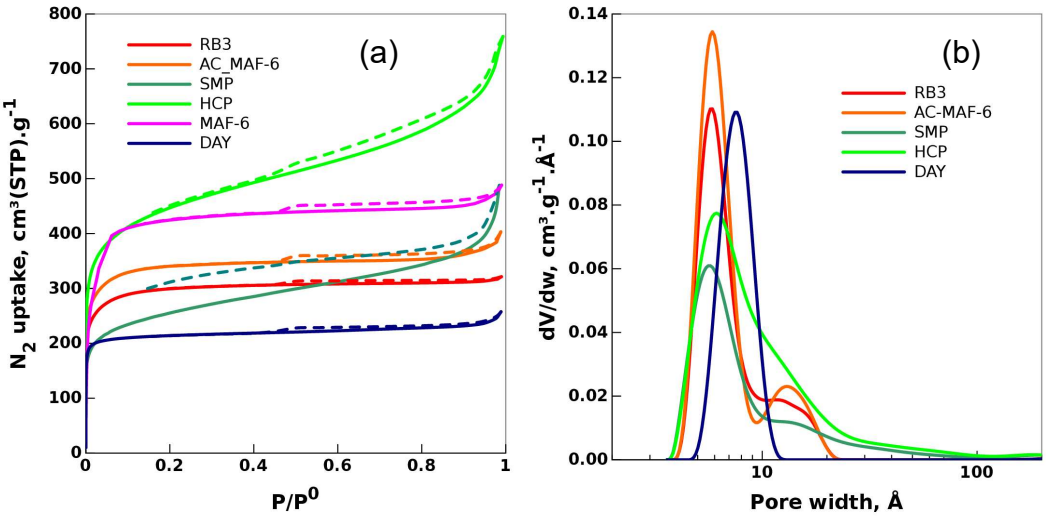

Figure 2 N_2 adsorption (full lines) and desorption (dotted lines) isotherms (77 K) of the sorbents studied in the work (a) and NLDFT pore size distributions for Norit RB3, AC-MAF-6, HCP, SMP and DAY (b).

To characterize the pore size in the used sorbents two different approaches were employed. The used version of SAIEUS software does not allow to determine the pore size distribution for MOFs from N_2 adsorption isotherms. Therefore, for MAF-6 we used the crystallographic data according to which this sorbent contains well defined spherical cavities separated by the apertures of 7.6 Å [28]. For other

sorbents the NLDFT calculations allowed to obtain their pore size distribution (PSD) (Fig.2b). For DAY the maximum of the pore size distribution determined by NLDFT (7.5 Å) is very close to the size calculated from its crystalline structure (7.4 Å [42]). In polymers and activated carbons the main peak in micropore range is located at ~ 6 Å. In active carbons another peak in PSD is observed between 10 and 20 Å. In polymers larger pores are also present whose sizes show a continuous distribution from 6 up to 300 Å confirming their micro and mesoporous nature.

3.2. Adsorption isotherms

Water adsorption

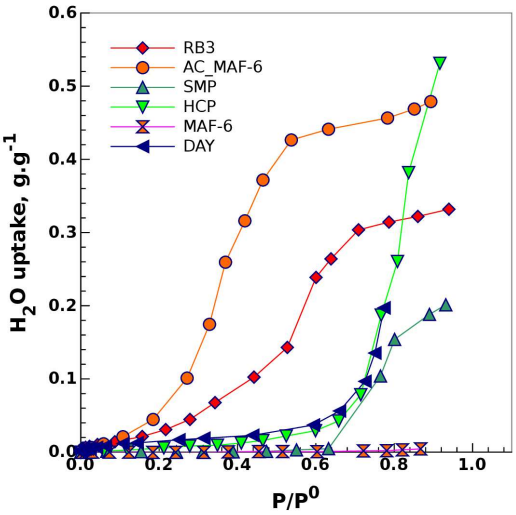

Figure 3 H_2O adsorption isotherms measured at 25 °C.

Water vapor, omnipresent in ambient air, can strongly compete with toluene molecules during their adsorption. Given the weakly polar character of toluene, the hydrophobic sorbents should be more selective in toluene adsorption under humid conditions. To characterize hydrophobicity we measured water adsorption isotherms at 25°C (Fig.3). It follows that MAF-6 stands apart from other materials since it is fully hydrophobic showing only negligible water adsorption up to $P/P^0 = 0.9$. The other

materials are less hydrophobic than MAF-6 and show different water uptakes which depend strongly on water vapor pressure.

The polymers HCP, SMP and the DAY zeolite are quite hydrophobic for $P/P^0 < 0.6$ since their water capacities in this pressure range are smaller than 0.03 $g.g^{-1}$. In contrast, above $P/P^0 = 0.6$ water adsorption isotherm shows a steep rise achieving the highest adsorbed amount in HCP (0.53 $g.g^{-1}$ at $P/P^0 = 0.92$) due to water condensation in the mesopores (Fig.3). The active carbons (Norit RB3 and AC-MAF-6) demonstrate low water adsorption for $P/P^0 < 0.2$: less than 0.03 $g.g^{-1}$ for Norit RB3 and 0.06 $g.g^{-1}$ for AC-MAF-6. However under conditions typical for ambient air ($0.2 < P/P^0 < 0.6$) they adsorb much higher amounts of water: 0.13 $g.g^{-1}$ for Norit RB3 and 0.40 $g.g^{-1}$ for AC-MAF-6 at $P/P^0 = 0.5$. The smaller water uptake by Norit RB3 carbon reflects less polar character of its surface which is due to a lower oxygen content and absence of nitrogen atoms on the surface of this material. It is worth noting that despite the presence of oxygen on their surface, HCP and SMP materials are more hydrophobic than carbons for $0.2 < P/P^0 < 0.6$. This effect can be due to a less polar character of the oxygen-containing groups and/or to their lower accessibility in the polymers.

Toluene adsorption isotherms

The complete toluene adsorption isotherms are given in Fig.4. For active carbons, DAY and MAF-6 the isotherms are of Type I showing a behavior typical for rigid microporous sorbents: initial increase of amount adsorbed is followed by a saturation plateau (Fig.4a). The toluene adsorbed volume corresponding to this plateau is close to the micropore volume (Table S1). In contrast, for SMP and HCP after the initial adsorption stage below 1 hPa, corresponding to micropores filling, the toluene uptake continues to increase. This effect originates from two phenomena. First, it reflects the filling of mesopores present in HCP and SMP materials. Second, given a polymer nature of these sorbents, this increase can also be due to a swelling process in which the toluene molecules fill the intermolecular space between the polymer chains [25]. This swelling phenomenon is clearly seen in

SMP material in which the maximum adsorbed volume of toluene exceeds the total pore volume measured from N_2 adsorption isotherm. Thus, SMP adsorbs 1.1 $cm^3.g^{-1}$ of toluene at 37.2 hPa (P/P^0 = 0.99) while the total pore volume calculated from N_2 adsorption isotherm is equal to 0.93 $cm^3.g^{-1}$.

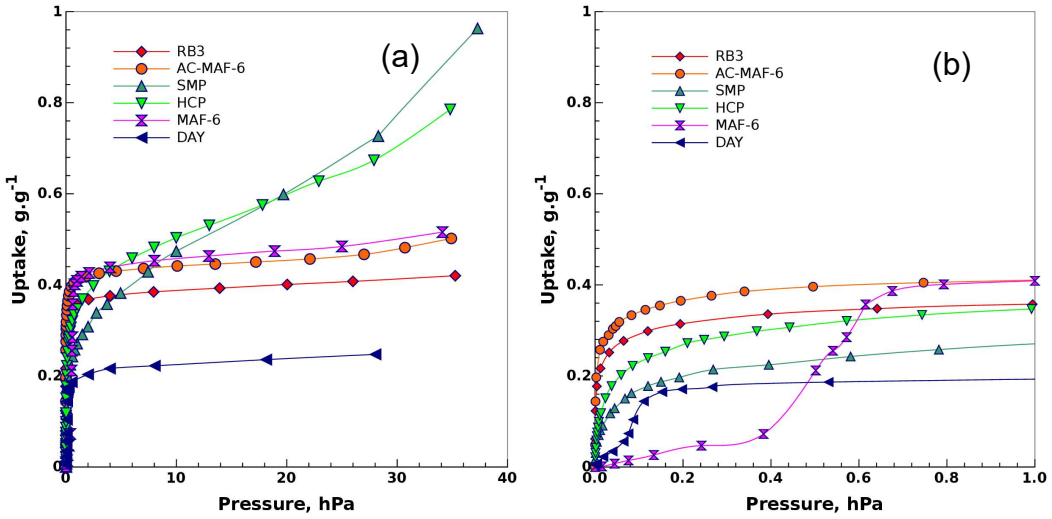

Figure 4 Toluene adsorption isotherms at 25 °C: full pressure range (a) and low-pressure range (< 1 hPa) (b). The lines are the guides for the eye.

In the low-pressure range of toluene adsorption isotherm (Fig.4b) the behavior of DAY and MAF-6 differs from the other materials. In contrast to the activated carbons and polymers the isotherms of DAY and MAF-6 at low pressure are of convex shape (associated with Type III isotherms). In these materials the toluene adsorption isotherms are therefore not of simple type, but have a composite nature (I and III). The convex shape of adsorption isotherm is characteristic of the systems in which the adsorbate-adsorbate interactions are stronger than adsorbate-adsorbent interactions [36]. The particular properties of MAF-6 and DAY at low toluene pressure can thus be attributed to weak interactions of toluene molecules with the surface at low pressure. In the case of MAF-6 the presence of a steep increase of the adsorbed amount at 0.4 hPa can also be due to the "gate opening" phenomenon frequently observed in MOFs [43]. Even if the nominal aperture size in this structure (7.6 Å) is larger than the size of toluene molecule (5.3 Å), the true aperture size in an empty structure can be smaller because of its flexibility. In such a case pore filling becomes possible only after a

certain threshold pressure is reached at which the presence of adsorbed species allows the "gate opening" in the structure. The small uptake of toluene at low pressure observed in DAY and MAF-6 suggests that these two materials are not suitable for capturing toluene when its pressure is below 10 Pa (~ 100 ppm), despite a favorable toluene/water separation ratio in these sorbents (see Table S2).

The aim of the present study is to evaluate the performance of the sorbents for toluene capture in ambient air at low concentration. The capacities down to 0.1 Pa (~ 1 ppm) can be accurately measured in our thermobalance (Table 3). To estimate the capacities at lower toluene pressure we fitted the measured isotherms and calculated the adsorbed amount by extrapolation. To do so one cannot use the approach based on the potential theory of Polanyi (Dubinin-Astakhov equation) since the corresponding isotherm does not have the thermodynamically consistent (linear) behavior at the zero-pressure limit [44]. Therefore, to estimate the uptakes below 0.1 Pa we fitted the low- pressure part of the isotherms (< 100 Pa) using the Unilan equation which has a correct behavior in the zero-pressure limit [44]:

$$N = \frac{N_m}{2s} ln\left(\frac{1+be^{s}p}{1+be^{-s}p}\right) \quad (1)$$

where N is the adsorbed amount, N_m is the maximum adsorbed amount, s is the heterogeneity parameter, b is the equilibrium constant, p is the pressure. It can be shown [44] that in the zero pressure limit the uptake becomes a linear function of pressure with the Henry constant equal to:

$$H = N_m b\left(\frac{sinhs}{s}\right) \quad (2)$$

where *sinh s* is the hyperbolic sinus of s.

The optimized fit parameters for the most promising materials (Norit RB3, AC-MAF-6, SMP and HCP) are presented in Table 3. Fig.5 shows that these parameters describe correctly the behavior of

the isotherms in the low-pressure range. The Unilan equation (1) can therefore be used to estimate the toluene uptakes in this range which is not accessible experimentally (last column in Table 3).

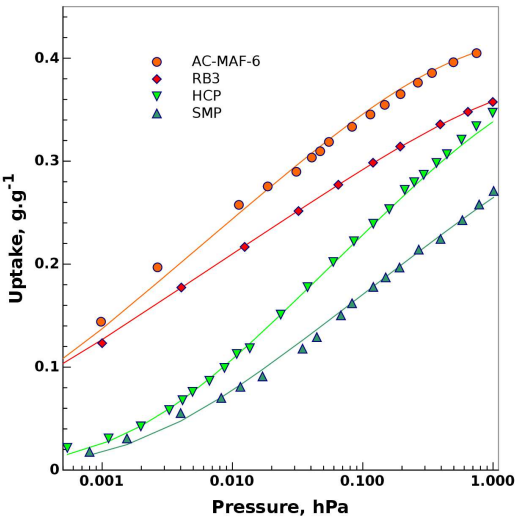

Figure 5 Low-pressure part of the toluene adsorption isotherms at 25 °C (log pressure scale) for Norit RB3, AC-MAF-6, HCP and SMP samples. The lines are the fits with the Unilan equation using the parameters given in Table 3.

Table 3 Optimal fitting parameters based on Unilan equation of the toluene adsorption isotherms for pressure below 1 hPa and adsorption capacities in the low-pressure range.

	Maximum amount adsorbed N_m, $g.g^{-1}$	Equilibrium constant b, Pa^{-1}	Heterogeneity parameter s	Henry constant, H, $g.g^{-1}.hPa^{-1}$	Uptake at 0.1 Pa $mg.g^{-1}$, **experimental**	Uptake at 0.01 Pa $mg.g^{-1}$, extrapolated
Norit RB3	0.39	1.50	5.3	1106	**123**	51
AC-MAF-6	0.43	1.86	4.5	800	**146**	47
SMP	0.35	0.09	4	22	**21**	2
HCP	0.40	0.17	3.5	40	**30**	3
MAF-6[a]					**0.2**	
DAY[a]					**5**	

[a] The Unilan equation is not applicable to these sorbents due to a convex shape of their isotherms at low pressure.

The large values of parameter *s* in the Unilan equation (1) suggest that all adsorbents are highly heterogeneous in toluene adsorption. Analysis of the data given in Table 3 shows that at 0.1 Pa the activated carbons adsorb much more toluene than the hyper-cross-linked polymers. Despite the

presence of aromatic rings and similar pore size the interaction of toluene molecules with surface appears weaker in polymers than in activated carbons. This effect can be attributed to a difference in the structure of pore walls in these classes of sorbents. In activated carbons the graphite like planes are rigid and form slit-shaped pores whose walls interact strongly with toluene molecules. In contrast, in hyper-cross-linked polymers due to flexibility of the polymer chains the aromatic rings present in their structure are not aligned in planes. The interaction of toluene molecules with such disordered walls should be less strong than with the flat walls present in activated carbons.

3.3. Breakthrough curves measurements

The breakthrough curves under dry conditions (Fig.6a) and the corresponding data (Table 4, Fig.S6) show that the stoichiometric sorbent capacities are similar to the equilibrium toluene uptakes obtained from the adsorption isotherms. Another parameter, breakthrough capacity, depends both on the equilibrium uptake and on the rate of mass transfer in the sorbent bed. These two capacities (breakthrough and stoichiometric) can be combined to estimate the overall efficiency of the sorbent under dynamic conditions in the form of the length of unused bed (LUB) [45]:

$$LUB = \left(1 - \frac{Q_{bt}}{Q_{st}}\right) L \quad (3)$$

where Q_{st} is the stoichiometric capacity, Q_{bt} is the breakthrough capacity and L is the bed length. Given that we used the same bed length for measuring all breakthrough curves, this parameter can be further simplified to obtain the fraction of unused bed (FUB):

$$FUB = 1 - \frac{Q_{bt}}{Q_{st}} \quad (4)$$

FUB describes quantitatively the steepness of a breakthrough curve and depends on the rate of mass transfer from the gas phase to the pores. A higher diffusion rate results in a steeper increase in the concentration and therefore in a lower FUB, which represents one of the main goals of the adsorption bed design.

Table 4 Toluene breakthrough and stoichiometric capacities obtained for 10 Pa of toluene under dry and humid conditions.

	Breakthrough capacity Q_{bt}, $g.g^{-1}$		Stoichiometric capacity Q_{st}, $g.g^{-1}$		Fraction of unused bed		Equilibrium uptake at 10 Pa, $g.g^{-1}$
	0% RH	50% RH	0% RH	50% RH	0% RH	50% RH	
Norit RB3	0.30	0.24	0.33	0.27	0.09	0.11	0.30
AC-MAF-6	0.22	0.19	0.37	0.30	0.41	0.37	0.34
SMP	0.11	0.086	0.20	0.19	0.45	0.55	0.17
HCP	0.21	0.15	0.29	0.26	0.28	0.42	0.24
MAF-6	0.008	0.008	0.026	0.026	0.67	0.65	0.022
DAY	0.067	0.036	0.17	0.13	0.61	0.72	0.14

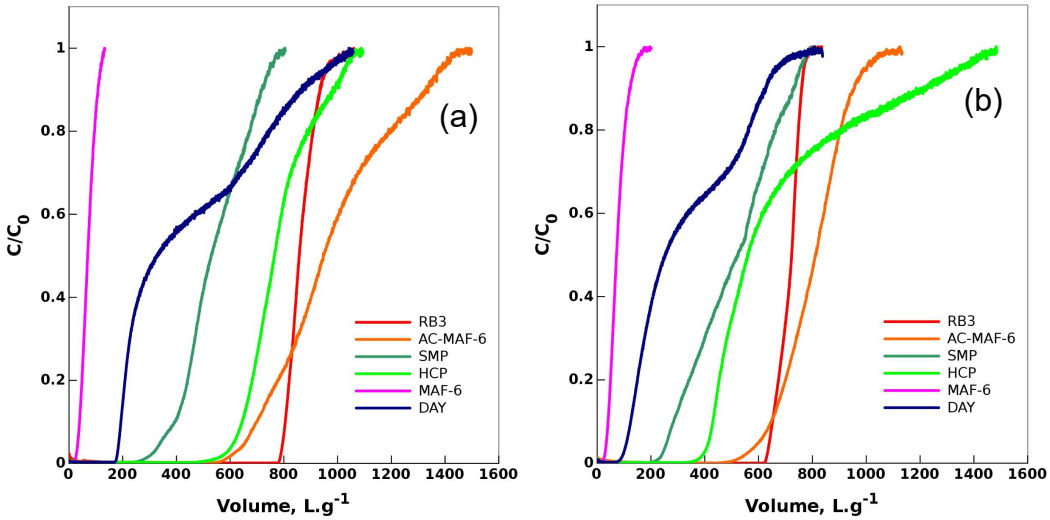

Figure 6 Breakthrough curves measured at 10 Pa of toluene at 25 °C under dry conditions (a) and at 50 % relative humidity (b).

Considering the stoichiometric capacity and the fraction of unused bed, the studied materials can be divided into three groups. The first one comprises the two least effective sorbents, MAF-6 and DAY. They have low adsorption capacities and high FUB because of the slow diffusion. This effect can be due to a combination of a small pore size (~ 7.4 Å) and exclusively microporous nature of these sorbents. Also, in the case of DAY the used shaping procedure (compaction of powder) was probably not an optimal one for providing a fast intercrystalline diffusion. The second group of sorbents

contains the hyper-cross-linked polymers and AC-MAF-6 carbon which show better performance than MAF-6 and DAY. The enhancement of bed utilization in this group originates possibly from faster mass transfer because of the presence of meso- and macropores in addition to micropores as follows from N_2 adsorption isotherms and SEM images of these samples. AC-MAF-6 does not contain mesopores, but assemblage of the well-defined particles (see Fig.S4) in the adsorbent bed should create interparticle voids whose presence enhances the toluene transfer. Finally, the best sorbent, Norit RB3 activated carbon, shows both the high capacity and very low fraction of unused bed. This performance is not surprising given the highly optimized textural properties of this material which has been used on the industrial scale for decades.

Despite lower capacities of the novel materials in comparison with Norit RB3, we consider that there is a room for their improvement. Thus, in the case of AC-MAF-6 the appropriate treatment of the material can be used to create mesopores, e.g. by annealing with KOH [46]. Such modification will enhance the diffusion of guest molecules and allow consequently to increase its breakthrough capacity. For hyper-cross-linked polymers the use of other monomers (through co-polymerization) could be envisaged to increase the rigidity of the structure. This approach could allow to improve both their affinity for aromatic molecules and their transport properties.

The presence of humidity (50% RH) in the gas flow affects the performance of all sorbents to varying extent as it was previously observed for other types of VOC sorbents [47] (Fig.6b and Table 4). As expected, the most hydrophilic material, AC-MAF-6, shows the strongest decrease of the stoichiometric capacity (19%) due to a pronounced adsorption competition between toluene and water molecules. It is worth noting however that despite this decrease, the stoichiometric capacity of AC-MAF-6 in the presence of water is similar to that of RB3 which is less hydrophilic. The hydrophobic materials show only a small decrease of 5 - 10% (for SMP and HCP) or preserve their stoichiometric capacity intact as it is the case for MAF-6.

The breakthrough capacity under humid conditions also declines for all sorbents except MAF-6. The magnitude of this decrease depends however on the type of adsorbent. As shown in Fig.S7, for RB3 and AC-MAF-6 the stoichiometric and breakthrough capacities decrease to a similar extent (15 – 20%). In contrast, for the other materials (HCP, SMP and DAY) the breakthrough capacity is affected by the water vapor much more strongly than their stoichiometric capacity. For example, in the case of HCP addition of water vapor results in 30% decrease of the breakthrough capacity, while the stoichiometric capacity loses only 10% of its value. This fact points out that in these solids water molecules influence not only the overall capacity due to adsorption competition with toluene, but also the toluene diffusion. This observation is rather unexpected given that these materials adsorb only very small amounts of water at 50% RH (see Fig.3). We suppose that the adsorbed water molecules can be localized on some special adsorption sites (e.g. at the pore aperture) which allow them to slow down the toluene diffusion despite a small adsorbed amount. This observation shows that prediction of sorbent performance under humid conditions by extrapolation from water free measurements can be unreliable even for strongly hydrophobic materials.

We would like to note that ideally the dynamic adsorption capacities of different sorbents should be compared using materials in the same form (powder or agglomerates). It is not the case in the present study in which AC-MAF-6, HCP, SMP and MAF-6 were used in a powdered form while Norit RB3 and DAY were studied as agglomerates. The reason for this approach is that the development of the shaping procedure of novel materials is a difficult task which could not be addressed in the present work. We consider however that our comparative analysis of the dynamic adsorption properties remains meaningful. In fact, the role of a correct shaping procedure is to create agglomerates in which the transport properties of a powdered material are fully preserved. We may consider therefore that the properties of the novel materials revealed in our study are the best properties which can be achieved for these materials and which will be preserved if their shaping is done correctly.

3.4. Desorption of toluene and regenerability of the sorbents

Despite a complex shape of the desorption curves (Fig.7), it can be observed that the facility of desorption of toluene varies strongly in the studied materials. Thus, for RB3 and AC-MAF-6 the maximum of concentration is observed at ~ 130 °C and the desorption process extends up to 300 °C. In contrast, in the case of HCP and DAY the maximum is located at ~ 75 °C and desorption of toluene is completed below 200 °C. As can be expected the lowest desorption temperature (~ 40 °C) is observed for MAF-6. This difference reflects the much stronger interaction of the toluene molecules with the surface of the activated carbons, which is in line with the values of the Henry constants (Table 3).

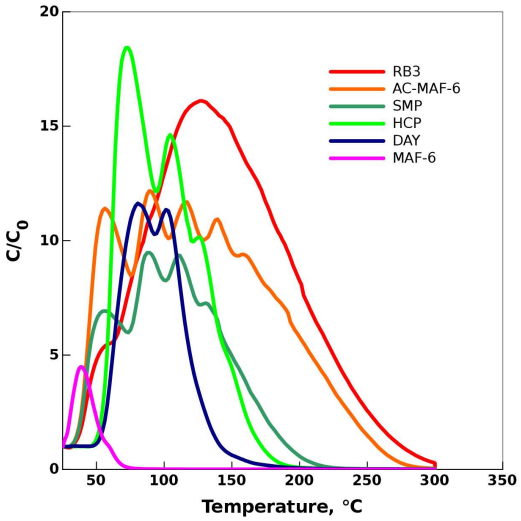

Figure 7 Toluene thermal desorption curves under N_2 flow (temperature ramp – 10 °/min).

The observed difference in toluene desorption behavior has important practical implications. It follows that the used hyper-cross-linked polymers and DAY can be regenerated under milder conditions and more rapidly than the activated carbons. Also, a faster desorption allows to realize this stage with a smaller gas volume and to obtain therefore a more concentrated flow of the adsorbed species. This effect brings an advantage when the adsorbed species are recovered or when the sorbent is used as a preconcentrator of the species for their further analysis [48-50].

Regenerability is a key property of any sorbent. The use on industrial scale of activated carbons as Norit RB3 and zeolites as DAY certifies their high stability during regeneration under moderate temperatures (200 – 300 °C) and our data confirms the stability of these materials after several regeneration treatments at 200 °C (Fig.S8a,b). The same behavior is observed for AC-MAF-6 and MAF-6 samples (Fig.S8c,d) showing that the adsorption capacities of these novel materials are also fully preserved after several regeneration stages.

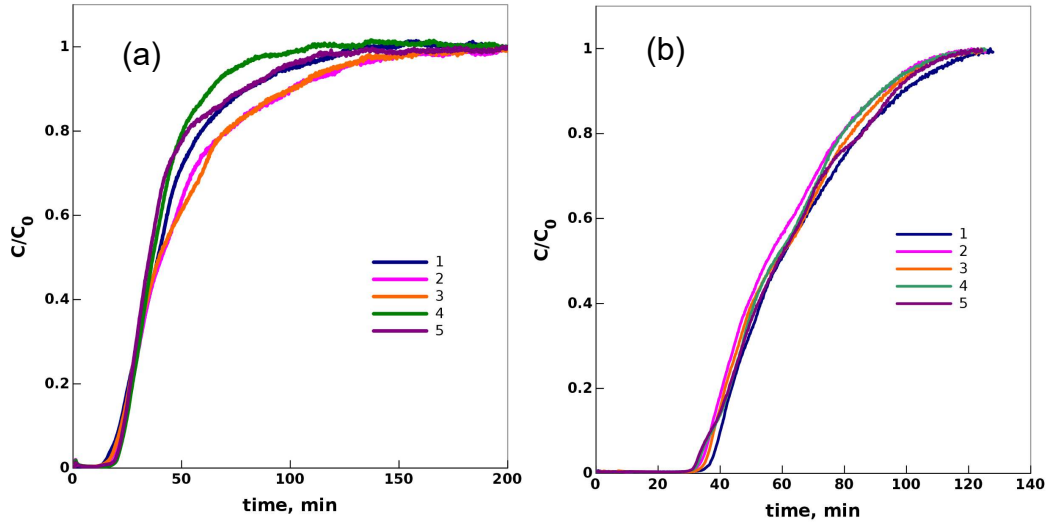

Figure 8 Five successive breakthrough curves for HCP (a) and SMP (b) samples under 10 Pa of toluene and 50% of RH (the sorbents were regenerated after each adsorption experiment under 20 % O_2 – 80 % N_2 flow for 4 h at 200 °C).

Despite the polymer nature of SMP and HCP materials, they maintain their adsorption capacity after regeneration at 200 °C in successive toluene adsorption/desorption cycles (Fig.8). Slight differences between the curves observed for HCP can be attributed to variation of the gas flow pattern in the adsorbent bed which consists of a non-shaped powdered sorbent. Despite this variation it can be concluded that the toluene adsorption capacity remains constant during cycling which confirms the full regenerability of SMP and HCP hyper-cross-linked polymers after toluene adsorption.

Conclusions

In the present work we studied the properties of novel porous materials in capture of toluene under humid conditions. The following materials were studied: MAF-6 MOF, hyper-cross-linked polymers (HCP and SMP) and AC-MAF-6, a MAF-6-derived activated carbon. For comparison purposes two conventional hydrophobic sorbents, Norit RB3 activated carbon and dealuminated Y zeolite (DAY), were also included in the study. The properties of the sorbents were characterized by measuring toluene and water adsorption isotherms and by recording breakthrough curves at 10 Pa of toluene under dry and humid (50% RH) conditions. The adsorption capacities at sub-ppm concentration range were evaluated by extrapolation of the toluene adsorption isotherms using the thermodynamically consistent Unilan model. The toluene desorption was characterized and the regenerability of all materials was confirmed.

We found that performances of MAF-6 are poor under the used conditions due to a weak affinity for toluene molecules at low pressure as shown by its adsorption isotherm. In contrast, other novel materials, AC-MAF-6 and HCP, demonstrate better performance. Thus, the stoichiometric capacities observed for AC-MAF-6 (0.30 g/g) and HCP (0.26 g/g) at 10 Pa of toluene and 50% of RH are close to that of Norit RB3 (0.27 g/g), a material used for VOC capture on the industrial scale. In terms of breakthrough capacity, the novel materials are less efficient than Norit RB3: the toluene breakthrough capacities for HCP (0.15 g/g) and AC-MAF-6 (0.19 g/g) are lower than that for Norit RB3 (0.24 g/g). It should be noted however that Norit RB3 has been used for decades while the novel materials were prepared only recently and their properties can be further improved. We consider thus that MOF-derived activated carbons and hyper-cross-linked polymers bear a strong potential for capture of aromatic VOCs under humid conditions.

Acknowledgements

We thank EUR EIPHI and Bourgogne Franche-Comté Region for financial support in the framework of DECOLAIR project. QP thanks European fund FEDER for financial support of his PhD project. SG, AK and LB gratefully acknowledge the Federal Ministry of Education and Research (Bundesministerium für Bildung und Forschung, BMBF) for support of the Mechanocarb project (award number 03SF0498). The help of F. Herbst (SEM) and of A. Krystianiak and O. Heintz (XPS measurements) is gratefully acknowledged.

References

1. E. M. Fujita, D. E. Campbell, B. Zielinska, W. P. Arnott, J. C. Chow Concentrations of Air Toxics in Motor Vehicle–Dominated Environments, Health Effect Institute Research Report, 156 (2011).
2. A.L. Bolden, C.F. Kwiatkowski, T. Colborn, New Look at BTEX: Are Ambient Levels a Problem? Environ. Sci. & Tech. 49 (2015) 5261–5276. https://doi.org/10.1021/es505316f.
3. T.M. Sack, D.H. Steele, K. Hammerstrom, J. Remmers, A survey of household products for volatile organic compounds, Atmos. Environ. Part A. Gen. Topics. 26 (1992) 1063–1070. https://doi.org/10.1016/0960-1686(92)90038-M.
4. L. Fishbein, An overview of environmental and toxicological aspects of aromatic hydrocarbons I.Benzene, Sci. Total Environ. 40 (1984) 189 – 218.
5. L. Fishbein, An overview of environmental and toxicological aspects of aromatic hydrocarbons II. Toluene, Sci. Total Environ. 42 (1985) 267–288. https://doi.org/10.1016/0048-9697(85)90062-2.
6. L. Fishbein, An overview of environmental and toxicological aspects of aromatic hydrocarbons III. Xylene, Sci. Total Environ. 43 (1985) 165–183. https://doi.org/10.1016/0048-9697(85)90039-7.
7. L. Fishbein, An overview of environmental and toxicological aspects of aromatic hydrocarbons IV. Ethylbenzene, Sci. Total Environ. 44 (1985) 269–287. https://doi.org/10.1016/0048-9697(85)90100-7.
8. IARC Working Group on the Evaluation of Carcinogenic Risks to Humans, ed., Overall evaluations of carcinogenicity: an updating of IARC monographs volumes 1 to 42. World Health Organization, International Agency for Research on Cancer, Lyon, France: Geneva, Switzerland, 1987.
9. C. Yang, G. Miao, Y. Pi, Q. Xia, J. Wu, Z. Li, J. Xiao, Abatement of various types of VOCs by adsorption/catalytic oxidation: A review, Chem. Eng. J. 370 (2019) 1128–1153. https://doi.org/10.1016/j.cej.2019.03.232.
10. X. Li, L. Zhang, Z. Yang, P. Wang, Y. Yan, J. Ran Adsorption materials for volatile organic compounds (VOCs) and the key factors for VOCs adsorption process: A review, Sep. Purif. Technol. 235 (2020) 116213. https://doi.org/10.1016/j.seppur.2019.116213
11. K. Vikrant, C.-J. Na, S.A. Younis, K.-H. Kim, S. Kumar, Evidence for superiority of conventional adsorbents in the sorptive removal of gaseous benzene under real-world conditions: Test of activated carbon against novel metal-organic frameworks, J. Clean. Prod. 235 (2019) 1090–1102. https://doi.org/10.1016/j.jclepro.2019.07.038.
12. C.K. Meininghaus, R. Prins, Sorption of volatile organic compounds on hydrophobic zeolites, Microporous and Mesoporous Mater. 35–36 (2000) 349–365. https://doi.org/10.1016/S1387-1811(99)00233-4.
13. M. Kraus, U. Trommler, F. Holzer, F.-D. Kopinke, U. Roland, Competing adsorption of toluene and water on various zeolites, Chem. Eng. J. 351 (2018) 356–363. https://doi.org/10.1016/j.cej.2018.06.128.
14. B.S. Bal'zhinimaev, E.A. Paukshtis, A.V. Toktarev, E.V. Kovalyov, M.A. Yaranova, A.E. Smirnov, S. Stompel, Effect of water on toluene adsorption over high silica zeolites, Microporous and Mesoporous Mater. 277 (2019) 70–77. https://doi.org/10.1016/j.micromeso.2018.10.023.
15. T. Yin, X. Meng, L. Jin, C. Yang, N. Liu, L. Shi, Prepared hydrophobic Y zeolite for adsorbing toluene in humid environment, Microporous and Mesoporous Mater. 305 (2020) 110327. https://doi.org/10.1016/j.micromeso.2020.110327.
16. C. Lai, Z. Wang, L. Qin, Y. Fu, B. Li, M. Zhang, S. Liu, L. Li, H. Yi, X. Liu, X. Zhou, N. An, Z. An, X. Shi, C. Feng, Metal-organic frameworks as burgeoning materials for the capture and

sensing of indoor VOCs and radon gases, Coord. Chem. Rev. 427 (2021) 213565. https://doi.org/10.1016/j.ccr.2020.213565.
17. K. Vellingiri, J.E. Szulejko, P. Kumar, E.E. Kwon, K.-H. Kim, A. Deep, D.W. Boukhvalov, R.J.C. Brown, Metal organic frameworks as sorption media for volatile and semi-volatile organic compounds at ambient conditions, Sci. Rep. 6 (2016). https://doi.org/10.1038/srep27813.
18. K. Vellingiri, P. Kumar, A. Deep, K.-H. Kim, Metal-organic frameworks for the adsorption of gaseous toluene under ambient temperature and pressure, Chem. Eng. J. 307 (2017) 1116–1126. https://doi.org/10.1016/j.cej.2016.09.012.
19. B.N. Bhadra, A. Vinu, C. Serre, S.H. Jhung, MOF-derived carbonaceous materials enriched with nitrogen: Preparation and applications in adsorption and catalysis, Mater. Today 25 (2019) 88–111. https://doi.org/10.1016/j.mattod.2018.10.016.
20. X. Zheng, Z. Wu, J. Yang, S. Rehman, R. Cao, P. Zhang, Metal–Organic Gel Derived N-Doped Granular Carbon: Remarkable Toluene Uptake and Rapid Regeneration, ACS Appl. Mater. Interfaces 13 (2021) 17543–17553. https://doi.org/10.1021/acsami.1c01524.
21. Z. Li, Y. Yuan, H. Wu, X. Li, M. Yuan, H. Wang, X. Wu, S. Liu, X. Zheng, M. Kim, H. Zheng, S. Rehman, G. Jiang, W. Fu, J. Jiang, Investigation of MOF-derived humidity-proof hierarchical porous carbon frameworks as highly-selective toluene absorbents and sensing materials, J. Hazard. Mater. 411 (2021) 125034. https://doi.org/10.1016/j.jhazmat.2020.125034.
22. W.-Q. Wang, J. Wang, J.-G. Chen, X.-S. Fan, Z.-T. Liu, Z.-W. Liu, J. Jiang, Z. Hao, Synthesis of novel hyper-cross-linked polymers as adsorbent for removing organic pollutants from humid streams, Chem. Eng. J. 281 (2015) 34–41. https://doi.org/10.1016/j.cej.2015.06.095.
23. R. Vinodh, E.M. Jung, M. Ganesh, M.M. Peng, A. Abidov, M. Palanichamy, W.S. Cha, H.T. Jang, Novel microporous hypercross-linked polymers as sorbent for volatile organic compounds and CO_2 adsorption, J. Ind. Eng. Chem. 21 (2015) 1231–1238. https://doi.org/10.1016/j.jiec.2014.05.039.
24. J. Wang, W.-Q. Wang, Z. Hao, G. Wang, Y. Li, J.-G. Chen, M. Li, J. Cheng, Z.-T. Liu, A superhydrophobic hyper-cross-linked polymer synthesized at room temperature used as an efficient adsorbent for volatile organic compounds, RSC Adv. 6 (2016) 97048–97054. https://doi.org/10.1039/C6RA18687D.
25. G. Paul, F. Begni, A. Melicchio, G. Golemme, C. Bisio, D. Marchi, M. Cossi, L. Marchese, G. Gatti, Hyper-Cross-Linked Polymers for the Capture of Aromatic Volatile Compounds, ACS Appl. Polym. Mater. 2 (2020) 647–658. https://doi.org/10.1021/acsapm.9b01000.
26. L. Lan, Y. Huang, Y. Dan, L. Jiang, Conjugated porous polymers for gaseous toluene adsorption in humid atmosphere, React. Funct. Polym. 159 (2021) 104804. https://doi.org/10.1016/j.reactfunctpolym.2020.104804.
27. J.-R. Li, R.J. Kuppler, H.-C. Zhou, Selective gas adsorption and separation in metal–organic frameworks, Chem. Soc. Rev. 38 (2009) 1477. https://doi.org/10.1039/b802426j.
28. C.-T. He, L. Jiang, Z.-M. Ye, R. Krishna, Z.-S. Zhong, P.-Q. Liao, J. Xu, G. Ouyang, J.-P. Zhang, X.-M. Chen, Exceptional Hydrophobicity of a Large-Pore Metal–Organic Zeolite, J. Amer. Chem. Soc.. 137 (2015) 7217–7223. https://doi.org/10.1021/jacs.5b03727.
29. S. Grätz, S. Zink, H. Kraffczyk, M. Rose, L. Borchardt, Mechanochemical synthesis of hyper-crosslinked polymers: influences on their pore structure and adsorption behaviour for organic vapors, Beilstein J. Org. Chem. 15 (2019) 1154–1161. https://doi.org/10.3762/bjoc.15.112.
30. A. Krusenbaum, S. Grätz, S. Bimmermann, S. Hutsch, L. Borchardt, The mechanochemical Scholl reaction as a versatile synthesis tool for the solvent-free generation of microporous polymers, RSC Advances. 10 (2020) 25509–25516. https://doi.org/10.1039/D0RA05279E.
31. B.N. Bhadra, J.Y. Song, S.-K. Lee, Y.K. Hwang, S.H. Jhung, Adsorptive removal of aromatic hydrocarbons from water over metal azolate framework-6-derived carbons, J. Hazard. Mater. 344 (2018) 1069–1077. https://doi.org/10.1016/j.jhazmat.2017.11.057.

32. B.N. Bhadra, S.H. Jhung, A remarkable adsorbent for removal of contaminants of emerging concern from water: Porous carbon derived from metal azolate framework-6, J. Hazard. Mater. 340 (2017) 179–188. https://doi.org/10.1016/j.jhazmat.2017.07.011.
33. M. Yuan, M. Gao, Q. Shi, J. Dong, Understanding the characteristics of water adsorption in zeolitic imidazolate framework-derived porous carbon materials, Chem. Eng. J. 379 (2020) 122412. https://doi.org/10.1016/j.cej.2019.122412.
34. K.-H. Kim, J.E. Szulejko, N. Raza, V. Kumar, K. Vikrant, D.C.W. Tsang, N.S. Bolan, Y.S. Ok, A. Khan, Identifying the best materials for the removal of airborne toluene based on performance metrics - A critical review, J. Clean. Prod. 241 (2019) 118408. https://doi.org/10.1016/j.jclepro.2019.118408.
35. J.E. Szulejko, K.-H. Kim, J. Parise, Seeking the most powerful and practical real-world sorbents for gaseous benzene as a representative volatile organic compound based on performance metrics, Sep. Purif. Technol. 212 (2019) 980–985. https://doi.org/10.1016/j.seppur.2018.11.001.
36. F. Rouquerol, J. Rouquerol, K.S.W. Sing, G. Maurin, P. Llewellyn, Adsorption by Powders and Porous Solids, Elsevier, 2014.
37. J. Jagiello, Stable Numerical Solution of the Adsorption Integral Equation Using Splines, Langmuir 10 (1994) 2778–2785. https://doi.org/10.1021/la00020a045.
38. N. Fairley, V. Fernandez, M. Richard-Plouet, C. Guillot-Deudon, J. Walton, E. Smith, D. Flahaut, M. Greiner, M. Biesinger, S. Tougaard, D. Morgan, J. Baltrusaitis, Systematic and collaborative approach to problem solving using X-ray photoelectron spectroscopy, Appl. Surf. Sci. Adv. 5 (2021) 100112. https://doi.org/10.1016/j.apsadv.2021.100112.
39. G. Gregis, S. Schaefer, J.-B. Sanchez, V. Fierro, F. Berger, I. Bezverkhyy, G. Weber, J.-P. Bellat, A. Celzard, Characterization of materials toward toluene traces detection for air quality monitoring and lung cancer diagnosis, Mater. Chem. Phys. 192 (2017) 374–382. https://doi.org/10.1016/j.matchemphys.2017.02.015.
40. S. Biniak, G. Szymański, J. Siedlewski, A. Świątkowski, The characterization of activated carbons with oxygen and nitrogen surface groups, Carbon. 35 (1997) 1799–1810. https://doi.org/10.1016/S0008-6223(97)00096-1.
41. NIST X-ray Photoelectron Spectroscopy Database, NIST Standard Reference Database Number 20, National Institute of Standards and Technology, Gaithersburg MD, 20899 (2000), doi:10.18434/T4T88K, (retrieved 14 january 2022).
42. R.T. Yang, Adsorbents: fundamentals and applications, Wiley-Interscience, Hoboken, N.J, 2003.
43. S. Horike, S. Shimomura, S. Kitagawa, Soft porous crystals, Nature Chem. 1 (2009) 695–704. https://doi.org/10.1038/nchem.444.
44. D.D. Do, Adsorption analysis: equilibria and kinetics, Imperial College Press, London, 1998.
45. W.J. Thomas, B.D. Crittenden, Adsorption technology and design, Butterworth-Heinemann, Oxford; Boston, 1998.
46. H.J. An, B.N. Bhadra, N.A. Khan, S.H. Jhung Adsorptive removal of wide range of pharmaceutical and personal care products from water by using metal azolate framework-6-derived porous carbon, Chem. Eng. J. 343 (2018) 447 – 554 https://doi.org/10.1016/j.cej.2018.03.025
47. E. Hunter-Stellars, J.J. Tee, I.P. Parkin, D.R. Williams Adsorption of volatile organic compounds by industrial porous materials: Impact of relative humidity, Microporous Mesoporous Mater. 298 (2020) 110090 https://doi.org/10.1016/j.micromeso.2020.110090.
48. M. Rieger, M. Wittek, P. Scherer, S. Löbbecke, K. Müller-Buschbaum, Preconcentration of Nitroalkanes with Archetype Metal-Organic Frameworks (MOFs) as Concept for a Sensitive Sensing of Explosives in the Gas Phase, Adv. Funct. Mater. 28 (2018) 1704250. https://doi.org/10.1002/adfm.201704250.

49. Y. Mohsen, H. Lahlou, J.-B. Sanchez, F. Berger, I. Bezverkhyy, G. Weber, J.-P. Bellat, Development of a micro-analytical prototype for selective trace detection of orthonitrotoluene, Microchem. J. 114 (2014) 48–52. https://doi.org/10.1016/j.microc.2013.12.001.
50. G. Gregis, J.-B. Sanchez, I. Bezverkhyy, W. Guy, F. Berger, V. Fierro, J.-P. Bellat, A. Celzard, Detection and quantification of lung cancer biomarkers by a micro-analytical device using a single metal oxide-based gas sensor, Sens. Actuators B: Chem. 255 (2018) 391–400. https://doi.org/10.1016/j.snb.2017.08.056.